Journal of the Australian Ceramic Society (2024) 60:399–406
https://doi.org/10.1007/s41779-023-00954-z

RESEARCH

A method of fabrication of porous carbonate apatite artificial bone for biomedical application

Xuan Thanh Tram Nguyen[1,2] · **Xuan Thang Cao**[3] · **Ishikawa Kunio**[4]

Received: 6 June 2023 / Revised: 5 September 2023 / Accepted: 16 September 2023 / Published online: 4 October 2023

Abstract

Among the various bone substitutes, carbonate apatite (CO_3Ap) has received significant attention in the field of hard tissue regeneration due to its similarity in chemical composition to natural bone and its osteoconductivity and bioresorbability. This study aimed to develop a cost-effective method for fabricating porous CO_3Ap blocks while maintaining a balance between porosity and mechanical properties. The level of interconnectivity in the porous structure was achieved by adjusting the pore volume fractions of the starting materials. The phase and microstructure characteristics of the porous CO_3Ap blocks were assessed using techniques such as X-ray diffraction (XRD), Fourier-transform infrared spectroscopy (FTIR), and scanning electron microscopy (SEM). The diametral tensile strength (DTS) of the blocks was determined using a universal testing machine. The results demonstrated that the mechanical strength of the blocks stayed within a range that was suitable for handling properties. This advantage allows the porous blocks to withstand initial stress during implantation procedures or in the early stages of defect healing.

Keywords Carbonate apatite · Interconnected pore · Dissolution–precipitation · Mechanical strength

Introduction

Congenital defects, trauma, carcinogens, and accidents can cause damage to hard tissues. While bone has the ability to regenerate, it often requires significant time and may not always achieve proper healing. In cases where natural therapies fail to promote remodeling, bone grafting is utilized to replace the damaged tissues through regeneration. Porous carbonate apatite (CO_3Ap) materials are particularly appealing as bone substitutes due to their similar structure and inorganic composition to human cancellous bone. These materials offer several advantages, including the stimulation of osteoblast cells responsible for bone formation and osteoclast cells responsible for bone resorption. This stimulation promotes the beneficial process of bone remodeling and aids in the regeneration of lost or damaged bone tissue [1–13].

Over time, porous CO_3Ap materials have garnered increasing attention as a viable approach for repairing bone defects. Extensive research has focused on improving their properties to strike a balance between mechanical strength and biological functionality. An interconnected porous structure is ideal for facilitating cell migration, nutrient exchange, fluid flow, and vascularization. However, achieving such a structure often comes at the expense of mechanical strength, as a trade-off exists where increased porosity results in reduced strength. Several methods exist for fabricating three-dimensional (3D) porous scaffolds, including foaming agent–based techniques, the polymeric sponge replica process, and templating methods [6, 10, 11, 14–27]. In the templating approach, a sacrificial template called a porogen is used, which is subsequently removed through thermal treatment or dissolution to create the desired porous structure. This method offers simplicity and advantages in producing interconnected pores with controllable sizes and shapes.

✉ Xuan Thanh Tram Nguyen
nxttram@hcmut.edu.vn

1 Division of Biomedical Engineering, Faculty of Applied Science, Ho Chi Minh City University of Technology, Ho Chi Minh City 70000, Vietnam

2 Vietnam National University Ho Chi Minh City, Linh Trung Ward, Thu Duc District, Ho Chi Minh City 70000, Vietnam

3 Faculty of Chemical Engineering, Industrial University of Ho Chi Minh City, Ho Chi Minh City 700000, Vietnam

4 Department of Biomaterials, Faculty of Dental Science, Kyushu University, Fukuoka, Japan

It should be noted that CO_3Ap materials are sensitive to elevated temperatures due to the decomposition of the carbonate group [2, 3, 28, 29]. Consequently, direct sintering cannot be employed to solidify CO_3Ap blocks. Instead, the dissolution and precipitation method [3, 17, 23–26, 30–33] shows promise in transforming calcium carbonate ($CaCO_3$) precursors into CO_3Ap blocks. $CaCO_3$, comprising calcium and carbonate, is an ideal precursor due to its low solubility in neutral solutions. Moreover, producing pure $CaCO_3$ blocks can be achieved by the reaction of calcium hydroxide ($Ca(OH)_2$) with carbon dioxide (CO_2). Ultimately, chemically pure CO_3Ap blocks are obtained through the phase transformation of $CaCO_3$ precursors in a phosphate salt solution. This method allows for the production of low-crystalline and bioactive CO_3Ap blocks that possess desirable biological properties.

In this study, a combination of the templating approach and the dissolution and precipitation method was employed to create a 3D porous CO_3Ap scaffold. The desired pore morphology and size for bone substitutes typically involve interconnected pores with diameters ranging from 100 to 400 µm [14, 34–42]. It is supposed that achieving a balance between porosity and mechanical strength in the CO_3Ap scaffold is a crucial criterion in this study to provide surgeons with better handling of the material of bone graft substitutes. In that case, it would be reasonable to propose a cost-effective method for fabricating the CO_3Ap scaffold for bone implant applications. The ultimate objective of this study is to explore the feasibility of such a method.

Materials and methods

Preparation

Calcium hydroxide ($Ca(OH)_2$, 2511–4400, Daejung Chemicals & Metals Co., Ltd, Gyeonggi-do, Korea) was firstly mixed with calcium sulfate hemihydrate ($CaSO_4.0.5H_2O$, 2522–4000, Daejung Chemicals & Metals Co., Ltd, Gyeonggi-do, Korea). The mixing ratio was varied from 50 to 100%wt. The NaCl granules (125–300 µm) were used as sacrificial templates in which the weight ratio of chemical powders/NaCl granules was 50:50. Blocks were prepared by uniaxial pressing with the compaction pressure as 15 MPa, 25 MPa, and 45 MPa. The compacted samples were kept at 37 °C for 24 h in a drying oven. In the next step, they were exposed to carbon dioxide (CO_2) gas with 0.2 L/min placed in a sealed container for 14 days. Next, they were soaked in 1 mol/L $NaHCO_3$ (7566–4400, Daejung Chemical & Metals Co. Ltd. Gyeonggi-do, Korea) solution at 60 °C for 48 h for the complete carbonation. Blocks were then washed and soaked in the distilled water at 60 °C for 48 h to eliminate entirely NaCl granules. Consequently, the porous blocks could be obtained, and they were then immersed in 1 mol/L Na_2HPO_4 (7613–4400, Daejung chemical & metals Co. Ltd. Gyeonggi-do, Korea) solution at 90 °C for 14 days for compositional phase transformation to final apatite phase. Finally, samples were taken out, rinsed with distilled water, and dried at 60 °C for 24 h before characterization. Samples were categorized according to the component of raw materials and the applied compaction pressure as shown in Table 1.

Phase characterization

The sample was ground to fine powder for Powder X-ray diffraction (XRD) analysis using a diffractometer system (D8 Advance, Bruker AXS GmbH, Karlsruhe, Germany). Vario1 Johansson focusing mono-chromator and high flux CuKα radiation generated at 40 kV and 40 mA were used for operation with scanning range from $2\theta = 10°$ to $2\theta = 60°$ (where θ is the Bragg angle) in a continuous mode. Fourier transform infrared spectrometer (FTIR) (InfraRed Bruker Tensor 37, Bruker AXS GmbH, Karlsruhe, Germany) analysis with KBr method was used to confirm the position of carbonate group in the apatite structure. Carbonate content was done by chemical analysis using CHN elemental analyzer (CHN coder MT-6, Yanaco, Japan).

Microstructure properties

Scanning electron microscope (SEM: S-3400N, Hitachi High-Technologies Co., Tokyo, Japan) at 10 kV of

Table 1 Type of samples

Sample	Weight ratio of chemical powders: NaCl granules	Component of chemical powders		Applied compaction pressure (MPa)
		$Ca(OH)_2$ (%wt)	$CaSO_4.0.5H_2O$ (%wt)	
50–50-15 MPa	50:50	50	50	15
50–100-15 MPa	50:50	100	0	15
50–50-25 MPa	50:50	50	50	25
50–100-25 MPa	50:50	100	0	25
50–50-45 MPa	50:50	50	50	45
50–100-45 MPa	50:50	100	0	45

accelerating voltage was used to analyze the structure and size of the pores. Sputter coating was employed to obtain high-quality images. The volume and weight of five samples were also measured for total porosity calculation.

Mechanical properties

Diametral tensile strength (DTS) value was collected using universal testing machine (AGS-J, Shimadzu Corporation, Kyoto, Japan). Five samples were tested to take the average DTS value.

Results and discussion

Figure 1 indicates XRD patterns of the samples (marked as 50–50-15 MPa, 50–100-15 MPa, 50–50-25 MPa, 50–100-25 MPa, 50–50-45 MPa, and 50–100-45 MPa) after carbonation, reference calcite, $Ca(OH)_2$, and $CaSO_4.2H_2O$ respectively. XRD pattern indicated that after carbonation, the compacted samples had main peaks at 2theta = 23, 29.5, and 39° belonging to calcite phase. However, the samples such as 50–100-15 MPa, 50–100-25 MPa, and 50–100-45 MPa, whose starting chemical ingredient is 100wt% $Ca(OH)_2$, possessed the minority species of $Ca(OH)_2$ with the existence of a weak peak at 2theta = 17.98°.

Figure 2 indicates XRD patterns of the samples (marked as 50–50-15 MPa, 50–100-15 MPa, 50–50-25 MPa, 50–100-25 MPa, 50–50-45 MPa, and 50–100-45 MPa) after immersing in Na_2HPO_4 1 mol/L at 90 °C for 14 days, reference hydroxyapatite (HAp), calcite, $Ca(OH)_2$, and

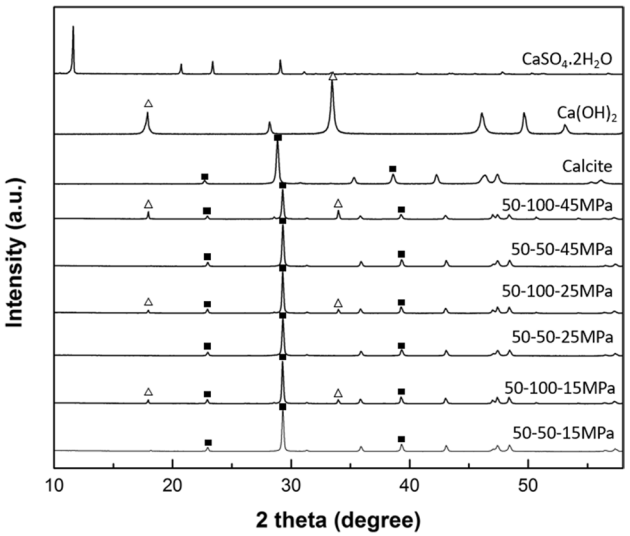

Fig. 1 XRD patterns of the compacted samples (marked as 50–50-15 MPa, 50–100-15 MPa, 50–50-25 MPa, 50–100-25 MPa, 50–50-45 MPa, and 50–100-45 MPa) after carbonation, reference calcite, $Ca(OH)_2$, and $CaSO_4.2H_2O$ respectively

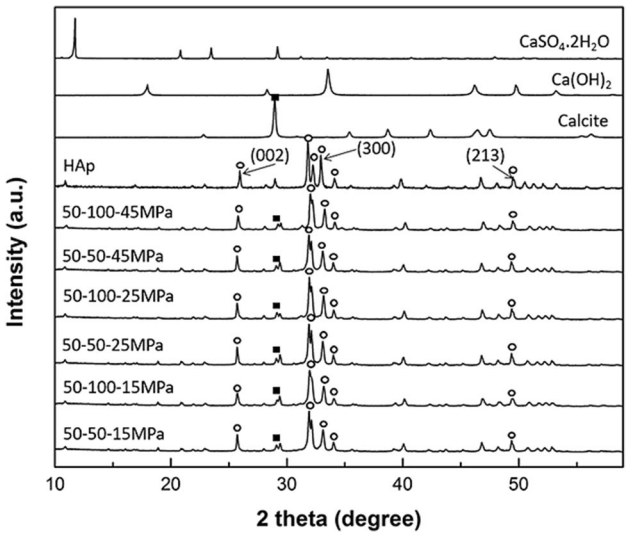

Fig. 2 XRD patterns of the porous (marked as 50–50-15 MPa, 50–100-15 MPa, 50–50-25 MPa, 50–100-25 MPa, 50–50-45 MPa, and 50–100-45 MPa) after immersing in Na_2HPO_4 1 mol/L at 90 °C for 14 days, reference hydroxyapatite (HAp), calcite, $Ca(OH)_2$, and $CaSO_4.2H_2O$ respectively

$CaSO_4{\cdot}2H_2O$ respectively. Main peaks of apatite phase were detected in all the XRD patterns of the samples as comparing to the ICDD standard peak of stoichiometric hydroxyapatite (standard no. 09–0432). The minority phase of calcite also existed with the detection of a weak peak at 2theta = 29.5°. Table 2 lists the lattice parameters of apatite crystals estimated using XRD data. It should be noted that the lattice parameter variation between stoichiometric HAp and carbonate apatite (CO_3Ap) was due to the introduction of carbonate group into the crystal structure. Low crystallinity of B-type CO_3Ap, the same component with natural bone, has the contraction of the *a*-axis and the expansion of the *c*-axis since the smaller (CO_3) groups substitute the larger (PO_4) tetrahedra. Therefore, the c/a ratio of B-type CO_3Ap is higher than that of standard HAp [3, 13, 43–45]. And hence, the obtained results indicated

Table 2 Lattice parameters from XRD data

Samples	Lattice parameters		
	a(Å)	c(Å)	c/a
Standard HAp (ICDD PDF card no. 9432)	9.4180	6.8840	0.7309
50–50-15 MPa	9.3715	6.9276	0.7392
50–100-15 MPa	9.3581	6.9244	0.7399
50–50-25 MPa	9.3785	6.9307	0.7390
50–100-25 MPa	9.3599	6.9327	0.7407
50–50-45 MPa	9.3774	6.9324	0.7393
50–100-45 MPa	9.3291	6.9102	0.7407

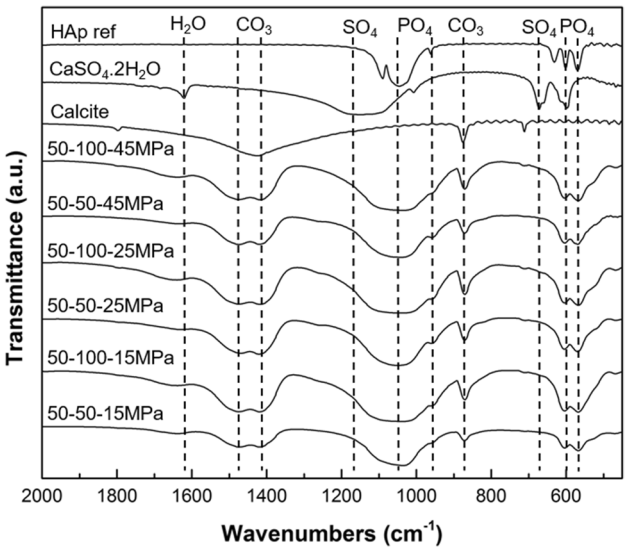

Fig. 3 FTIR spectra of the samples (marked as 50–50-15 MPa, 50–100-15 MPa, 50–50-25 MPa, 50–100-25 MPa, 50–50-45 MPa, and 50–100-45 MPa) after immersing in Na_2HPO_4 1 mol/L at 90 °C for 14 days, calcite, $CaSO_4{\cdot}2H_2O$, and reference hydroxyapatite (HAp) respectively

that all the samples were B-type CO_3Ap which owned the increase of the c/a ratio as shown in Table 2.

Figure 3 shows the FTIR spectra of the samples (marked as 50–50-15 MPa, 50–100-15 MPa, 50–50-25 MPa, 50–100-25 MPa, 50–50-45 MPa, and 50–100-45 MPa) after immersing in Na_2HPO_4 1 mol/L at 90 °C for 14 days, calcite, $CaSO_4{\cdot}2H_2O$, and reference hydroxyapatite (HAp), respectively. FTIR spectra of all samples exhibited the characteristic peaks of the apatites such as the vibration of PO_4^{3-} group at wavenumber 980–1100 cm^{-1}, 960 cm^{-1}, and 560–600 cm^{-1}. When compared with the standard spectrum of HAp, it could be seen that CO_3Ap showed the difference in the presentation of the doublet peak at 1455–1410 cm^{-1} and singlet band at 875 cm^{-1} caused by the vibration of CO_3^{2-} group [2, 13, 32, 43, 44, 46] . Besides, the nonappearance of OH^- peak ở 630 cm^{-1} also supported that B-type CO_3Ap was the main phase of samples after phosphorization. This was in agreement with the estimation of lattice parameter by the above XRD results. These results and the carbonate content of CO_3Ap blocks measured by CHN analysis (as shown in Table 3) were used to confirm the location of the carbonate group in the apatite structure. The typical carbonate band of calcite at 712 cm^{-1} was neglected, and this implied that a very small amount of calcite precursor remained and the phase transformation from calcite to CO_3Ap was almost complete. The addition of $CaSO_4$ could accelerate the nucleation within disordered precursors, decrease the reaction time, and improve the phase transformation.

Table 3 Carbonate content of CO_3Ap blocks measured by CHN analysis ($p < 0.05$)

Samples	Carbonate content (mass %)
50–50-15 MPa	11.3 ± 0.3
50–100-15 MPa	11.1 ± 0.1
50–50-25 MPa	12.2 ± 0.3
50–100-25 MPa	13.8 ± 0.4
50–50-45 MPa	14.7 ± 0.2
50–100-45 MPa	10.6 ± 0.4

In this study, it proved that dissolution–precipitation reaction was suitable for fabrication of the CO_3Ap block. This CO_3Ap block maintained its macroscopic structure even when it passed through the compositional transformation. In short, $Ca(OH)_2$ absorbed the CO_2 gas and transformed to calcite then it dissolved in the phosphate solution and supplied Ca^{2+} and CO_3^{2-}. CO_3Ap was formed due to the supersaturation of the solution containing Ca^{2+}, CO_3^{2-}, and PO_4^{3-} with respect to CO_3Ap. The mechanism of this precipitation could be explained by the stable property of apatite phase in the neutral and basic conditions. It is noted that dissolution process must balance with precipitation reactions for the preservation of the precursor structure and the efficiency of the reaction. The fast dissolution might lead to the deterioration of sample whereas the low process would extend the reaction duration [3, 47].

Figures 4 and 5 show the morphology and distribution of pores in the bodies of the samples after carbonation and after immersing in Na_2HPO_4 1 mol/L at 90 °C for 14 days. The porous morphology appears as the network of interconnected pores. It also indicated that the architecture including size and shape of multiple channels with interconnected pores was not varied during the dissolution–precipitation reaction and phase transformation. The pore size ranging from 100 to 400 µm made the samples be suitable bone tissue engineering applications. Figure 6 demonstrates the total porosity of calcite precursor blocks formed by the carbonation and CO_3Ap formed by the compositional transformation using calcite blocks as precursors. The higher applied compaction pressure increased the density; consequently, the total porosity decreased. It was also found that the phase transformation to CO_3Ap resulted in increasing the total porosity except for the samples such as 50–50-25 MPa and 50–50-45 MPa which possessed the total porosity of the CO_3Ap blocks which was lower than that of the calcite precursor blocks. The change in the total porosity was closely related to the rate of phase transformation. Thereby, the interlocking of the precipitated CO_3Ap resulted in the transformation of calcite to CO_3Ap through dissolution–precipitation reactions while maintaining the macroscopic block structure.

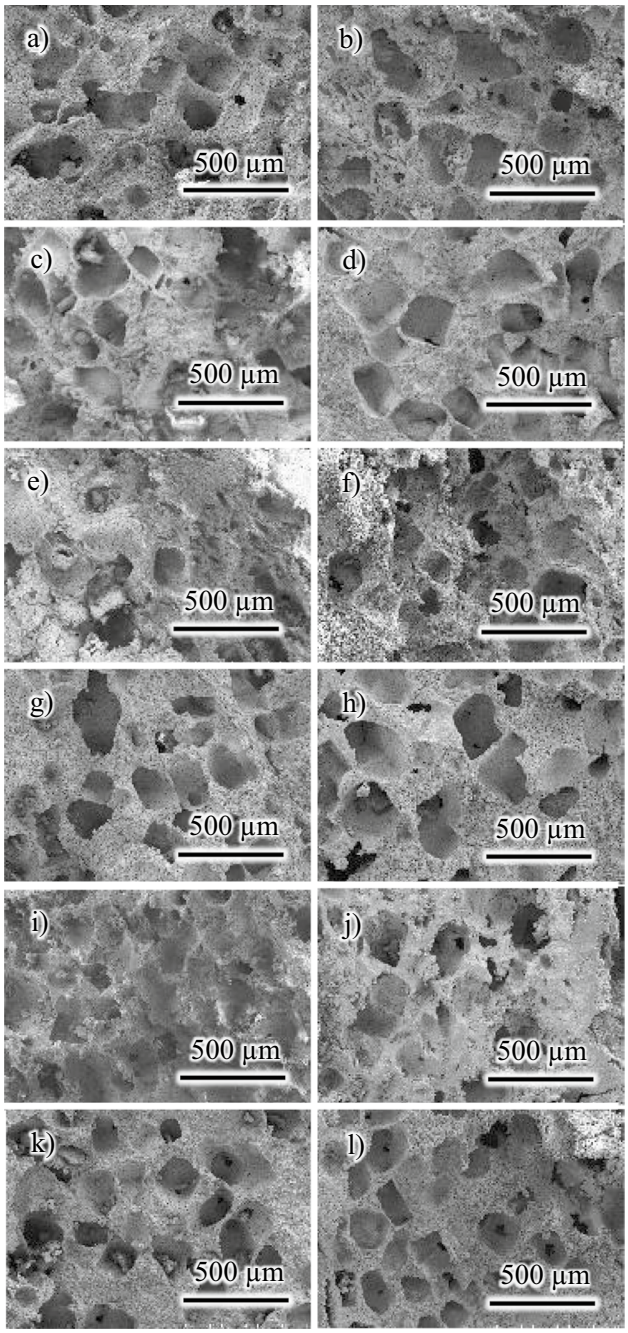

Fig. 4 SEM images of the fracture surfaces of the samples after carbonation [**a** 50–50-15 MPa, **c** 50–100-15 MPa, **e** 50–50-25 MPa, **g** 50–100-25 MPa, **i** 50–50-45 MPa, and **k** 50–100-45 MPa] and after immersing in Na_2HPO_4 1 mol/L at 90 °C for 14 days [**b** 50–50-15 MPa, **d** 50–100-15 MPa, **f** 50–50-25 MPa, **h** 50–100-25 MPa, **j** 50–50-45 MPa, and **l** 50–100-45 MPa]

The present study indicated that porous CO_3Ap blocks encountered the requirements of the porous bone implant, accordingly; the pore size of the obtained CO_3Ap blocks was between 100 and 400 µm and that was the optimal size for bone ingrowth. The biological and mechanical properties of the material are related to the porous architecture. The pore diameter ranging from 17.9 to 30.4 µm is suitable for the migration of mesenchymal stem cell [48, 49] ; in addition, the dramatically high proliferation, differentiation, and even gene expression can be encouraged in the pore range of 100–300 µm [43, 50].

Figure 7 summarizes the DTS values of the samples 50–50-15 MPa, 50–100-15 MPa, 50–50-25 MPa, 50–100-25 MPa, 50–50-45 MPa, and 50–100-45 MPa after carbonation and after immersing in Na_2HPO_4 1 mol/L at 90 °C for 14 days. The strength of the calcite block formed from $Ca(OH)_2$ and $CaSO_4$ precursor mixture was lower than that of the calcite block fabricated from pure $Ca(OH)_2$ block. On the contrary, after immersing in phosphate solution, the CO_3Ap samples obtained from precursors containing $CaSO_4$ had higher strength than the CO_3Ap samples with initial chemical composition of 100% mass $Ca(OH)_2$. This difference in DTS value of both samples is presumably related to the difference in phase composition as indicated by the XRD and FTIR results. Moreover, an increase in the compaction pressure caused an increase in the DTS value. However, the strength of the sample 50–100-45 MPa was observed to be lower as compared to that of the others compacted under lower pressure. The reason for this is due to the deformation under an applied hydraulic pressure such as cracks or even layer splitting. After transformation to CO_3Ap by immersing in Na_2HPO_4 1 mol/L at 90 °C for 14 days, the DTS values of the samples were approximately 0.5–4 MPa. This value would be probably acceptable for handling properties of bone substitutes.

The previous studies stated that porosity was inversely proportional to the strength in which the strength and durability of bone substitutes were considerably affected by pore size of greater than 100 µm [17, 31, 39, 51–54]. It should be noted that promoting the bone ingrowth and regeneration is the advantage of interconnecting porous structure; however, the dominance of large pores can significantly deteriorate the mechanical properties and threaten the implant stability. The current generation of bone-substituting materials should be equilibrium between the biological and mechanical properties for the effective hard tissue grafting. The obtained CO_3Ap block from the effective composition-transformation process had the proper mechanical strength satisfying the handling property of the porous bone implant; therefore, it could withstand the initial stress in the reconstructive surgeon. The $CaCO_3$ precursor transformed to the B-type CO_3Ap characterizing with the high content of carbonate that is equivalent to the natural human bone. Therefore, the CO_3Ap block in this study is expected to exhibit the same osteoconductivity and bioresorbability of human bone, while also promoting superior bone remodeling that contributes to bone healing over time.

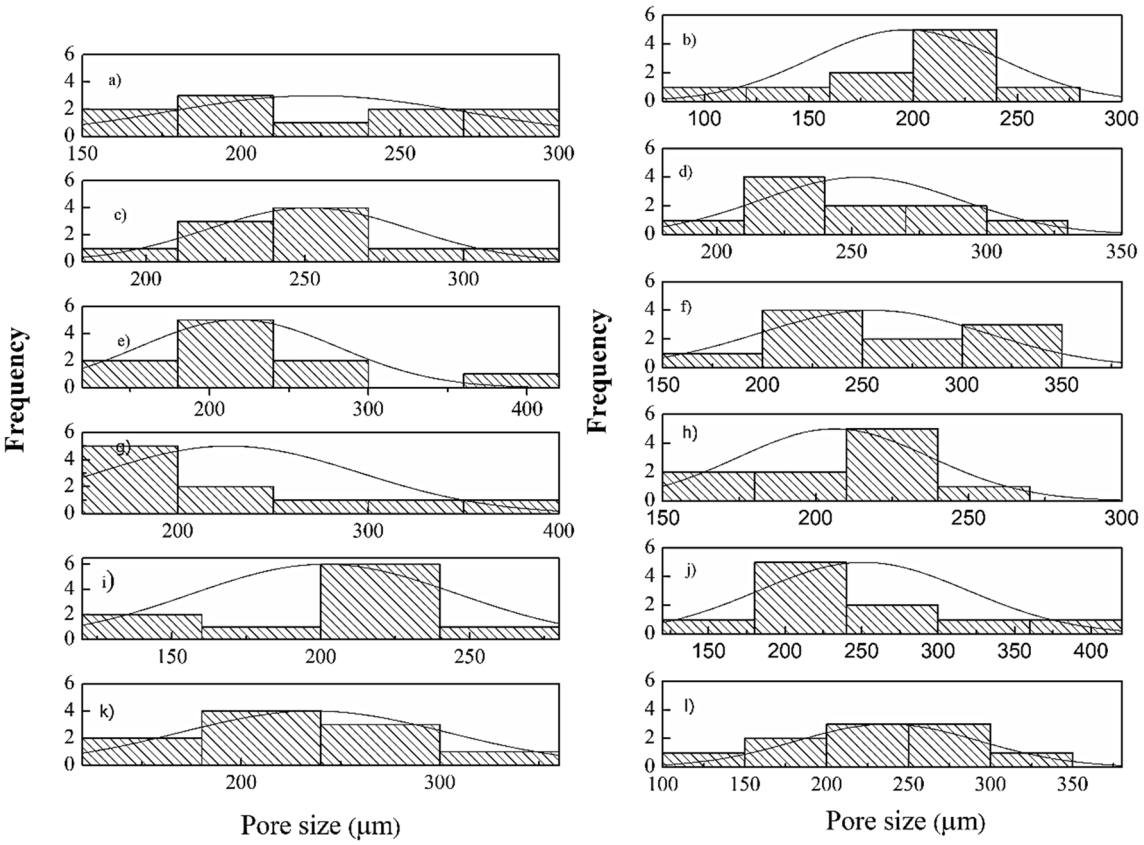

Fig. 5 The pore size distribution analysis of the samples after carbonation [(a) 50–50-15 MPa, (c) 50–100-15 MPa, (e) 50–50-25 MPa, (g) 50–100-25 MPa, (i) 50–50-45 MPa, and (k) 50–100-45 MPa] and after immersing in Na_2HPO_4 1 mol/L at 90 °C for 14 days [(b) 50–50-15 MPa, (d) 50–100-15 MPa, (f) 50–50-25 MPa, (h) 50–100-25 MPa, (j) 50–50-45 MPa, and (l) 50–100-45 MPa]

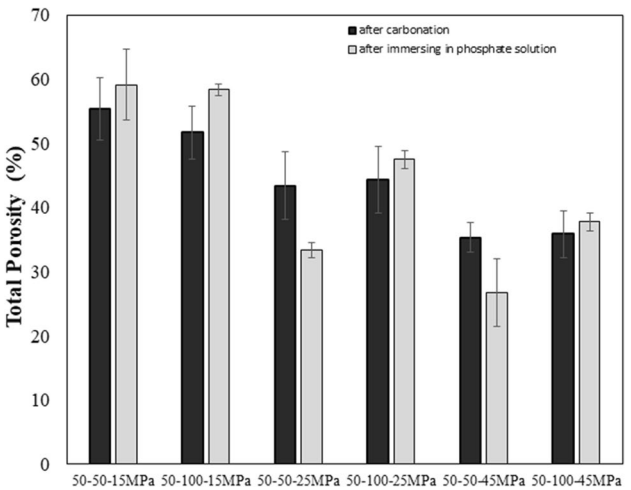

Fig. 6 The total porosity of the samples 50–50-15 MPa, 50–100-15 MPa, 50–50-25 MPa, 50–100-25 MPa, 50–50-45 MPa, and 50–100-45 MPa after carbonation (black column) and after immersing in Na_2HPO_4 1 mol/L at 90 °C for 14 days (grey column) ($p < 0.05$)

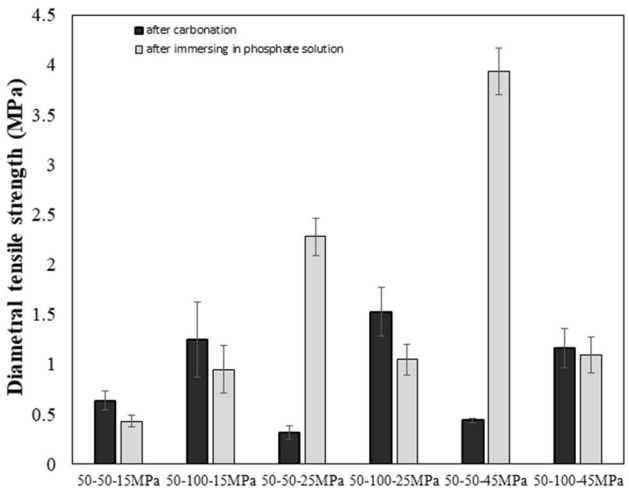

Fig. 7 Diametral tensile strength (DTS) of the samples 50–50-15 MPa, 50–100-15 MPa, 50–50-25 MPa, 50–100-25 MPa, 50–50-45 MPa, and 50–100-45 MPa after carbonation (black column) and after immersing in Na_2HPO_4 1 mol/L at 90 °C for 14 days (grey column) ($p < 0.05$)

Conclusion

In summary, the present study introduced a low-cost method for the preparation of porous CO_3Ap bone substitutes. The content and size of the NaCl porogen affects the interconnected microporous structure. This porous architecture was stable even when the sample is going through two phase transitions as showing in microscopic images. The mechanical properties of the CO_3Ap block are suitable for processing during implantation (0.5–4 MPa). The B-type CO_3Ap block was characterized with the high carbonate content in the structure similar to human bone. This bone replacement material is expected to provide a positive approach to improve the quality of bone defect treatment, especially for low-income patients in developing countries.

Acknowledgements We acknowledge the support of time and facilities from Ho Chi Minh City University of Technology (HCMUT) for this study.

Funding This research is funded by Vietnam National University Ho Chi Minh City (VNU-HCM) under grant number C-2022–20-24.

Declarations

Competing interests The authors declare no competing interests.

References

1. LeGeros, R.Z., Trautz, O.R., LeGeros, J.P., Klein, E., Shirra, W.P.: Apatite crystallites: effects of carbonate on morphology. Science. **155**(3768), 1409–1411 (1967). http://www.jstor.org/stable/1721190
2. Deguchi, K., Nomura, S., Tsuchiya, A., Takahashi, I., Ishikawa, K.: Effects of the carbonate content in carbonate apatite on bone replacement. J. Tissue Eng. Regen. Med. **16**(2), 200–206 (2022). https://doi.org/10.1002/term.3270
3. Ishikawa, K., Hayashi, K.: Carbonate apatite artificial bone. Sci. Technol. Adv. Mater. **22**(1), 683–694 (2021). https://doi.org/10.1080/14686996.2021.1947120
4. Hasegawa, M., Doi, Y., Uchida, A.: Cell-mediated bioresorption of sintered carbonate apatite in rabbits. J. Bone Joint Surg. - Series B. **85**(1), 142–147 (2003). https://doi.org/10.1302/0301-620X.85B1.13414
5. Cahyanto, A., Maruta, M., Tsuru, K., Matsuya, S., Ishikawa, K.: Fabrication of bone cement that fully transforms to carbonate apatite. Dent. Mater. J. **34**(3), 394–401 (2015). https://doi.org/10.4012/dmj.2014-328
6. Darus, F., Jaafar, M.: Enhancement of carbonate apatite scaffold properties with surface treatment and alginate and gelatine coating. J. Porous Mater. **27**(3), 831–842 (2020). https://doi.org/10.1007/s10934-019-00848-1
7. Madupalli, H., Pavan, B., Tecklenburg, M.M.J.: Carbonate substitution in the mineral component of bone: discriminating the structural changes, simultaneously imposed by carbonate in A and B sites of apatite. J. Solid State Chem. **255**, 27–35 (2017). https://doi.org/10.1016/j.jssc.2017.07.025
8. Kim, Y.S., Kwon, H.K., Kim, B.I.: Effect of nano-carbonate apatite to prevent re-stain after dental bleaching in vitro. J. Dent. **39**(9), 636–642 (2011). https://doi.org/10.1016/j.jdent.2011.07.002
9. Nagai, H., Kobayashi-Fujioka, M., Fujisawa, K., et al.: Effects of low crystalline carbonate apatite on proliferation and osteoblastic differentiation of human bone marrow cells. J Mater Sci: Mater Med. **26**, 99 (2015). https://doi.org/10.1007/s10856-015-5431-5
10 Hayashi, K., Yanagisawa, T., Shimabukuro, M., Kishida, R., Ishikawa, K.: Granular honeycomb scaffolds composed of carbonate apatite for simultaneous intra- and inter-granular osteogenesis and angiogenesis. Mater. Today Bio. **14**, 100247 (2022). https://doi.org/10.1016/j.mtbio.2022.100247
11. Keiichi, K., Mitsunobu, K., Masafumi, S., Yutaka, D., Toshiaki, S.: Induction of new bone by basic FGF-loaded porous carbonate apatite implants in femur defects in rats. Clin. Oral Implants Res. **20**(6), 560–565 (2009). https://doi.org/10.1111/j.1600-0501.2008.01676.x
12. Hafiyyah, O.A., Lastianny, S.P., Suryono.: Doxycycline incorporated in gelatin-carbonate apatite bone graft material: in vitro evaluation of osteoblastic alkaline phosphatase and porphyromonas gingivalis colonies. Malays. J. Med. Health. Sci. **16**(9), 57–61 (2020)
13. Tram, X.T.N., Ishikawa, K., Hoang Minh, T., Benson, D., Kanji, T.: Characterization of carbonate apatite derived from chicken bone and its in-vitro evaluation using MC3T3-E1 cells. Mater. Res. Express. **8**, 025401 (2021). https://doi.org/10.1088/2053-1591/abe018
14 Hayashi, K., Tsuchiya, A., Shimabukuro, M., Ishikawa, K.: Multiscale porous scaffolds constructed of carbonate apatite honeycomb granules for bone regeneration. Mater Des. **215**, 110468 (2022). https://doi.org/10.1016/j.matdes.2022.110468
15. Putri, T.S., Hayashi, K., Ishikawa, K.: Fabrication of three-dimensional interconnected porous blocks composed of robust carbonate apatite frameworks. Ceram. Int. **46**(12), 20045–20049 (2020). https://doi.org/10.1016/j.ceramint.2020.05.076
16. Keiichi, K., Mitsunobu, K., Masafumi, S., Yutaka, D., Toshiaki, S.: Induction of new bone by basic FGF-loaded porous carbonate apatite implants in femur defects in rats. Clin. Oral Implants Res. **20**(6), 560–565 (2009). https://doi.org/10.1111/j.1600-0501.2008.01676.x
17. Kishida, R., Elsheikh, M., Hayashi, K., Tsuchiya, A., Ishikawa, K.: Fabrication of highly interconnected porous carbonate apatite blocks based on the setting reaction of calcium sulfate hemihydrate granules. Ceram. Int. **47**(14), 19856–19863 (2021). https://doi.org/10.1016/j.ceramint.2021.03.324
18. Daitou, F., Maruta, M., Kawachi, G., et al.: Fabrication of carbonate apatite block based on internal dissolutionprecipitation reaction of dicalcium phosphate and calcium carbonate. Dent. Mater. J. **29**(3), 303–308 (2010). https://doi.org/10.4012/dmj.2009-095
19. Wakae, H., Takeuchi, A., Udoh, K., et al.: Fabrication of macroporous carbonate apatite foam by hydrothermal conversion of α-tricalcium phosphate in carbonate solutions. J. Biomed. Mater. Res. A **87**(4), 957–963 (2008). https://doi.org/10.1002/jbm.a.31620
20. Nomura, S., Tsuru, K., Maruta, M., Matsuya, S., Takahashi, I., Ishikawa, K.: Fabrication of carbonate apatite blocks from set gypsum based on dissolutionprecipitation reaction in phosphate-carbonate mixed solution. Dent. Mater. J. **33**(2), 166–172 (2014). https://doi.org/10.4012/dmj.2013-192
21 Hayashi, K., Kato, N., Kato, M., Ishikawa, K.: Impacts of channel direction on bone tissue engineering in 3D-printed carbonate apatite scaffolds. Mater Des. **204**, 109686 (2021). https://doi.org/10.1016/j.matdes.2021.109686
22. Ishikawa, K., Matsuya, S., Lin, X., Lei, Z., Yuasa, T., Miyamoto, Y.: Fabrication of low crystalline B-type carbonate apatite block from low crystalline calcite block. J. Ceram. Soc. Jpn. **118**(1377), 341–344 (2010). https://doi.org/10.2109/jcersj2.118.341
23. Ana, I.D., Matsuya, S., Ishikawa, K.: Engineering of carbonate apatite bone substitute based on composition-transformation of gypsum and calcium hydroxide. Engineering **02**(05), 344–352 (2010). https://doi.org/10.4236/eng.2010.25045

24. Maruta, M., Matsuya, S., Nakamura, S., Ishikawa, K.: Fabrication of low-crystalline carbonate apatite foam bone replacement based on phase transformation of calcite foam. Dent. Mater. J. **30**(1), 14–20 (2011). https://doi.org/10.4012/dmj.2010-087
25. Takeuchi, A., Munar, M.L., Wakae, H., et al.: Effect of temperature on crystallinity of carbonate apatite foam prepared from α-tricalcium phosphate by hydrothermal treatment. Biomed. Mater. Eng. **19**(2–3), 205–211 (2009). https://doi.org/10.3233/BME-2009-0581
26. Zaman, C.T., Takeuchi, A., Matsuya, S., Zaman, Q.H.M.S., Ishikawa, K.: Fabrication of B-type carbonate apatite blocks by the phosphorization of free-molding gypsum-calcite composite. Dent. Mater. J. **27**(5), 710–715 (2008). https://doi.org/10.4012/dmj.27.710
27. Ueno, H., Fujimi, T.J., Okada, I., Aizawa, M.: Development of biocompatible apatite sheets with various Ca/P ratios and carbonate ion contents for mouse osteoblastic cell culture and their evaluations. J. Aust. Ceram. Soc. **46**(2), 14–18 (2010)
28. Doi, Y., Shibutani, T., Moriwaki, Y., Kajimoto, T., Iwayama, Y.: Sintered carbonate apatites as bioresorbable bone substitutes. J Biomed Mater Res. **39**(4), 603–610 (1998). https://doi.org/10.1002/(SICI)1097-4636(19980315)39:4%3c603::AID-JBM15%3e3.0.CO;2-7
29. Koda, Y.D.T., Wakamatsu, N., Goto, T., et al.: Influence of carbonate on sintering of apatites. J. Dent. Res. **72**(9), 1279–1284 (1993). https://doi.org/10.1177/00220345930720090401
30. Lee, Y., Hahm, Y.M., Matsuya, S., Nakagawa, M., Ishikawa, K.: Characterization of macroporous carbonate-substituted hydroxyapatite bodies prepared in different phosphate solutions. J. Mater. Sci. **42**(18), 7843–7849 (2007). https://doi.org/10.1007/s10853-007-1629-3
31. Nomura, S., Tsuru, K., Maruta, M., Matsuya, S., Takahashi, I., Ishikawa, K.: Fabrication of carbonate apatite blocks from set gypsum based on dissolutionprecipitation reaction in phosphate-carbonate mixed solution. Dent. Mater. J. **33**(2), 166–172 (2014). https://doi.org/10.4012/dmj.2013-192
32. Lee, Y., Hahm, Y.M., Lee, D.H., Matsuya, S., Nakagawa, M., Ishikawa, K.: Preparation and characterization of macroporous carbonate-substituted hydroxyapatite scaffold. Ind. Eng. Chem. Res. **47**(8), 2618–2622 (2008). https://doi.org/10.1021/ie071474a
33. Daitou, F., Maruta, M., Kawachi, G., et al.: Fabrication of carbonate apatite block based on internal dissolutionprecipitation reaction of dicalcium phosphate and calcium carbonate. Dent. Mater. J. **29**(3), 303–308 (2010). https://doi.org/10.4012/dmj.2009-095
34. Jones, J.R., Lee, P.D., Hench, L.L.: Hierarchical porous materials for tissue engineering. Philos. Trans. Royal Soc. A: Math., Phys. Eng. Sci. **2006**(364), 263–281 (1838). https://doi.org/10.1098/rsta.2005.1689
35. Hollister, S.J.: Porous scaffold design for tissue engineering. Nat. Mater. **4**(7), 518–524 (2005). https://doi.org/10.1038/nmat1421
36. Jones, J.R., Hench, L.L.: Regeneration of trabecular bone using porous ceramics. Curr. Opin. Solid State Mater. Sci. **7**(4–5), 301–307 (2003). https://doi.org/10.1016/j.cossms.2003.09.012
37. Belyakov, A.V., Lukin, E.S., Safronova, T.V., Safina, M.N., Putlyaev, V.I.: Porous materials made from calcium phosphates (review). Glass and Ceramics (English translation of Steklo i Keramika). **65**(9–10), 337–339 (2008). https://doi.org/10.1007/s10717-009-9086-x
38. Will, J., Melcher, R., Treul, C., et al.: Porous ceramic bone scaffolds for vascularized bone tissue regeneration. J. Mater. Sci. Mater. Med. **19**(8), 2781–2790 (2008). https://doi.org/10.1007/s10856-007-3346-5
39. Abbasi, N., Hamlet, S., Love, R.M., Nguyen, N.T.: Porous scaffolds for bone regeneration. J. Sci.: Adv. Mater. Devices **5**(1), 1–9 (2020). https://doi.org/10.1016/j.jsamd.2020.01.007
40. Wu, R., Li, Y., Shen, M., et al.: Bone tissue regeneration: the role of finely tuned pore architecture of bioactive scaffolds before clinical translation. Bioact Mater. **6**(5), 1242–1254 (2021). https://doi.org/10.1016/j.bioactmat.2020.11.003
41. Perez, R.A., Mestres, G.: Role of pore size and morphology in musculo-skeletal tissue regeneration. Mater. Sci. Eng., C **61**, 922–939 (2016). https://doi.org/10.1016/j.msec.2015.12.087
42. Zhu, T., Cui, Y., Zhang, M., Zhao, D., Liu, G., Ding, J.: Engineered three-dimensional scaffolds for enhanced bone regeneration in osteonecrosis. Bioact Mater. **5**(3), 584–601 (2020). https://doi.org/10.1016/j.bioactmat.2020.04.008
43. Darus, F., Jaafar, M., Ahmad, N.: Preparation of carbonate apatite scaffolds using different carbonate solution and soaking time. Process. App. Ceram. **13**(2), 139–148 (2019). https://doi.org/10.2298/PAC1902139D
44. Ishikawa, K.: Carbonate apatite bone replacement: learn from the bone. J. Ceram. Soc. Jpn. **127**(9), 595–601 (2019). https://doi.org/10.2109/jcersj2.19042
45. Wang, B., Zhang, Z., Pan, H.: Bone apatite nanocrystal: crystalline structure, chemical composition, and architecture. Biomimetics. **8**(1), 90 (2023). https://doi.org/10.3390/biomimetics8010090
46. Murugan, R., Ramakrishna, S., Panduranga, R.K.: Nanoporous hydroxy-carbonate apatite scaffold made of natural bone. Mater. Lett. **60**(23), 2844–2847 (2006). https://doi.org/10.1016/j.matlet.2006.01.104
47. Ishikawa, K.: Bone substitute fabrication based on dissolution-precipitation reactions. Materials. **3**(2), 1138–1155 (2010). https://doi.org/10.3390/ma3021138
48. Ge, J., Guo, L., Wang, S., et al.: The size of mesenchymal stem cells is a significant cause of vascular obstructions and stroke. Stem Cell Rev Rep. **10**(2), 295–303 (2014). https://doi.org/10.1007/s12015-013-9492-x
49. Su, P., Tian, Y., Yang, C., Ma, X., Wang, X., Pei, J., Qian, A.: Mesenchymal stem cell migration during bone formation and bone diseases therapy. Int. J. Mol. Sci. **19**, 2343, (2018). https://doi.org/10.3390/ijms19082343
50. Matsiko, A., Gleeson, J.P., O'Brien, F.J.: Scaffold mean pore size influences mesenchymal stem cell chondrogenic differentiation and matrix deposition. Tissue Eng. Part A **21**(3–4), 486–497 (2015). https://doi.org/10.1089/ten.tea.2013.0545
51. Cyster, L.A., Grant, D.M., Howdle, S.M., et al.: The influence of dispersant concentration on the pore morphology of hydroxyapatite ceramics for bone tissue engineering. Biomaterials **26**(7), 697–702 (2005). https://doi.org/10.1016/j.biomaterials.2004.03.017
52. Akita, K., Fukuda, N., Kamada, K., et al.: Fabrication of porous carbonate apatite granules using microfiber and its histological evaluations in rabbit calvarial bone defects. J. Biomed. Mater. Res. A **108**(3), 709–721 (2020). https://doi.org/10.1002/jbm.a.36850
53. Baneshi, N., Moghadas, B.K., Adetunla, A., et al.: Investigation the mechanical properties of a novel multicomponent scaffold coated with a new bio-nanocomposite for bone tissue engineering: fabrication, simulation and characterization. J. Market. Res. **15**, 5526–5539 (2021). https://doi.org/10.1016/j.jmrt.2021.10.107
54. Yuliati, A., Merlindika, Y., Munadziroh, E., Ari, A., El Fadhlallah, M.P., Rianti, D., et al.: Mechanical strength and porosity of carbonate apatite-chitosan-gelatine scaffold in various ratio as a biomaterial candidate in tissue engineering. KEM. **829**, 173–81 (2019). https://doi.org/10.4028/www.scientific.net/KEM.829.173